

**Model Photospheres for Late-Type Stars from the Inversion of
High-Resolution Spectroscopic Observations. Groombridge 1830
and ϵ Eridani**

Carlos Allende Prieto

McDonald Observatory and Department of Astronomy,

The University of Texas at Austin

RLM 15.308, Austin, TX 78712-1083,

USA

Ramón J. García López

Instituto de Astrofísica de Canarias

E-38200, La Laguna, Tenerife,

SPAIN

David L. Lambert

McDonald Observatory and Department of Astronomy,

The University of Texas at Austin

RLM 15.308, Austin, TX 78712-1083,

USA

Basilio Ruiz Cobo

Instituto de Astrofísica de Canarias

E-38200, La Laguna, Tenerife,

SPAIN

Received _____; accepted _____

ABSTRACT

An inversion technique to recover LTE one-dimensional model photospheres for late-type stars, which was previously applied to the Sun (Allende Prieto et al. 1998), is now employed to reconstruct, semi-empirically, the photospheres of cooler dwarfs: the metal-poor Groombridge 1830 and the active star of solar-metallicity ϵ Eridani. The model atmospheres we find reproduce satisfactorily all the considered weak-to-moderate neutral lines of metals, satisfying in detail the excitation equilibrium of iron, the wings of strong lines, and the slope of the optical continuum. The retrieved models show a slightly steeper temperature gradient than flux-constant model atmospheres in the layers where $\log \tau \leq -0.5$. We argue that these differences should reflect missing ingredients in the flux-constant models and point to granular-like inhomogeneities as the best candidate.

The iron ionization equilibrium is well satisfied by the model for Gmb1830, but not for ϵ Eri, for which a discrepancy of 0.2 dex between the logarithmic iron abundance derived from neutral and singly ionized lines may signal departures from LTE. The chemical abundances of calcium, titanium, chromium, and iron derived with the empirical models from neutral lines do not differ much from previous analyses based on flux-constant atmospheric structures.

Subject headings: line: profiles – radiative transfer – stars: atmospheres – stars: late-type

1. Introduction

The measurement of chemical abundances from stellar spectra relies on a series of assumptions about the physical properties of the stellar atmosphere. Ideally a model atmosphere should be recoverable from the observed electromagnetic spectrum, but due to observational limitations models are either constructed from a few physical principles, that lead to a closed system of differential equations and boundary conditions, or modeled from some observed spectral features constrained by some theoretical bases. Such models are here referred to as theoretical and empirical (or semi-empirical) model atmospheres, respectively. The comparison between model atmospheres derived by different methods can be used to test our actual knowledge on the structure of the stellar atmosphere. Good agreement exists between theoretical and empirical models for the temperature stratification of the solar photosphere. Unlike the solar case, where the high quality of the spectroscopic observations has motivated both the empirical modeling and theoretical studies of its atmosphere, the analyses of more distant late-type stars are commonly carried out using relatively simple theoretical models for their photospheres. As an example, it is rare to find studies in the literature analyzing in detail the likely errors that occur when interpreting the stellar spectra with model atmospheres based on approximations such as Local Thermodynamical Equilibrium (LTE).

Previous efforts to model empirically the photospheres and chromospheres of cool stars others than the Sun, such as those by Mäckle et al. (1975) for Arcturus, Ruland et al. (1980) for Pollux, Magain (1985) for the metal poor sub-giant HD140283, or Thatcher et al. (1991) for ϵ Eri were severely limited by the quality of the spectroscopic observations. Technical advances in astronomical instrumentation have made it possible to acquire data more comparable to that for the Sun. Extremely high resolving power and signal-to-noise ratio is feasible for many stars, at least to seventh magnitude. In this environment, we

have reconsidered the possibility of semi-empirical modeling the photospheres of cool stars by developing an inversion code of stellar spectra. The method has been previously tested with the Sun (see Allende Prieto et al. 1998), demonstrating that it is able to recover the depth-stratification of the solar photosphere from **normalized** spectral line profiles. The procedure involves the assumption that the stellar photosphere is plane-parallel, in LTE, in steady state, and in hydrostatic equilibrium. The star is assumed to rotate as a solid body. Magnetic fields are neglected.

We have selected two well-known nearby stars for this study: the metal-poor G8 dwarf Gmb1830 (HD103095; HR4550; $[\text{Fe}/\text{H}]^1 \sim -1.3$) and the solar-like metallicity K2V ϵ Eri (HD22049; HR1084). Gmb1830 is the brightest star ($V = 6.42$) that is significantly metal deficient. It has been studied widely making use of theoretical model atmospheres and high resolution spectroscopic observations, e.g. Smith, Lambert, & Ruck (1992) and Balachandran & Carney (1996). The star was reported to show radial velocity variations (Beardsley, Gatewood, & Kamper 1974), but subsequent detailed studies (Griffin 1984; Heintz 1984) did not confirm the variations. The star shows a periodic variation of the emission in the Ca II H and K lines, likely reflecting a solar-like activity cycle with a period of about 7 years (Wilson 1978; Radick et al. 1998). ϵ Eri is a young and active dwarf surrounded by a ring of dust at a distance of 60 AU (Greaves et al. 1998). Its line bisectors, magnetic activity, and temperature have been observed to vary by Gray & Baliunas (1995).

We have obtained high-quality spectroscopic data for these stars and followed the inversion procedure previously applied to the Sun. Next section describes the observations and the database employed in the study. §3 describes the details of the inversion procedure, and §4 the retrieved model atmospheres and their comparison with observations, while §5

¹ $[\text{M}/\text{H}] = \log\left(\frac{N(\text{M})}{N(\text{H})}\right) - \log\left(\frac{N(\text{M})}{N(\text{H})}\right)_{\odot}$ where $N(\text{M})$ is the number density of the nuclei of the element M and "H" refers to hydrogen.

discusses and summarizes the main conclusions.

2. Observations of high resolution line profiles. Archived and previously published complementary spectroscopic information

Optical spectroscopic observations were carried out in 1996 February using the higher resolution camera of the *2dcoudé* echelle spectrograph (Tull et al. 1995) coupled to the Harlan J. Smith Telescope at McDonald Observatory (Mt. Locke, Texas). The cross-disperser and the availability of a 2048×2048 pixels CCD detector made it possible to gather up to 300 \AA in a single exposure. The set-up provided a resolving power of $\lambda/\Delta\lambda \simeq 200000$. As many 1/2 hour exposures were acquired as were needed to reach a signal to noise ratio (SNR) of $\sim 300\text{--}800$. Table 1 describes the observational program.

A very careful data reduction was applied using the IRAF² software package, and consisted of: overscan (bias) and scattered light subtraction, flatfielding, extraction of one-dimensional spectra, wavelength calibration and continuum normalization. Wavelength calibration was performed for each individual image using ~ 300 Th-Ar lines spread over the detector. The possibility of acquiring daylight spectra with the same spectrograph allowed us to perform a few interesting tests. Comparison of the wavelengths of 60 lines in a single daylight spectra (SNR $\sim 400\text{--}600$, depending on the spectral order) with the high accuracy wavelengths measured in the solar flux spectrum by Allende Prieto & García López (1998) showed that the rms difference was at the level of 58 m s^{-1} ($\sim \frac{1}{11}$ pixel). Before co-adding the individual one-dimensional spectra, they were first cross-correlated to

²IRAF is distributed by the National Optical Astronomy Observatories, which are operated by the Association of Universities for Research in Astronomy, Inc., under cooperative agreement with the National Science Foundation.

correct for the change in Doppler shifts and instrumental drifts. More details are given in Allende Prieto et al. (1999a).

Measurements of the optical continuum flux are available for the two stars, although the fluxes are not on an absolute scale. The Breger (1976) catalogue includes both stars, and Gmb1830 was also observed by Peterson & Carney (1979) and Carney (1983). The IUE³ satellite observed both stars, and their UV fluxes are on an absolute scale, providing complementary information, but as ϵ Eri is a chromospherically active star, its UV spectrum rich in emission lines is not adequate to study the star’s photosphere. The available spectra of Gmb1830 (Table 2) covering wavelengths redder than 2000 Å were critically compared, and averaged. The velocity shifts between individual spectra were found to be smaller than ~ 1 Å, unimportant so for the analysis of the continuum. Interstellar extinction was considered negligible.

3. Inversion

3.1. Trigonometric gravities and initial metallicities

The inversion code assumes hydrostatic equilibrium. Therefore, gravity must be known to attempt the inversion. The chemical abundances of the elements responsible for the atomic lines we use as input data are derived in the inversion process, but an initial appraisal of the overall chemical composition is necessary.

Following a procedure strictly identical to that applied by Allende Prieto et al. (1999b) to more than two hundred cool stars of different metallicities, we have derived the *trigonometric* gravities for the two nearby stars studied here from the *Hipparcos* parallaxes,

³The spectra were retrieved from the IUE Final Archive; Garhart et al. 1997.

finding $\log g = 4.68 \pm 0.07$ dex for Gmb1830 and 4.84 ± 0.07 dex for ϵ Eri. Spectroscopic studies assign to Gmb1830 metallicities in the range $-1.2 \leq [\text{Fe}/\text{H}] \leq -1.4$ (see Smith et al. 1992). Analyses of ϵ Eri point to slightly lower than solar metallicities, typically within $-0.2 \leq [\text{Fe}/\text{H}] \leq 0.0$ (Drake & Smith 1993).

3.2. Input data and inversion procedure

The line profiles entering the inversion code MISS (Multi-line Inversion of Stellar Spectra) were carefully selected following the same criteria employed for the solar case (Allende Prieto et al. 1998): they should be included in the compilation of solar lines by Meylan et al. (1993), their transition probabilities should have been measured by Blackwell and collaborators in Oxford (e.g. Blackwell & Shallis 1979), and they should be weaker than $80 \text{ m}\text{\AA}$ in equivalent width (W_λ), to minimize both departures from LTE, and the underestimate of the line damping by using the Unsöld approximation (see, e.g., Ryan 1998). These criteria provided 13 lines of iron, calcium, titanium, and chromium in the spectral range covered for Gmb1830, and 10 of them were also useful for ϵ Eri (the restriction of the lines' W_λ to be smaller than $80 \text{ m}\text{\AA}$ was slightly relaxed for ϵ Eri). This is a significantly smaller number of lines than the set employed for the solar inversion but, as we shall demonstrate below, the atmospheric structure can still be derived with confidence. The wings of the Ca I 6162 Å line were included, as discussed for the solar inversion by Allende Prieto et al. (1998), using the theoretical estimates of Spielfiedel et al. (1991) for the damping due to collisions with hydrogen atoms. The line data is listed in Table 3: all lines were used for the modeling of Gmb1830, and those employed for ϵ Eri are identified with an asterisk.

The inversion proceeds analogously to the solar case, starting from an isothermal model photosphere ($T = 5000 \text{ K}$), increasing progressively the number of nodes until either no

significant improvement in the fit of the line profiles is achieved or the temperature structure shows wiggles, which are evidence that the degree of the chosen polynomial is too high. The solar abundances (Anders & Grevesse 1989) were taken as starting point for ϵ Eri, while the abundances of the elements heavier than helium were scaled by a factor 0.0316 ($[M/H] = -1.5$) for Gmb1830. The abundances assumed at the beginning do not determine the final result. Fig. 1 shows the evolution of the iron abundance through the inversion procedure for Gmb1830, assuming different initial guesses. An initial iron abundance that was more than ~ 0.3 dex from $[Fe/H] = -1.5$ provided a significantly different final abundance and a model photosphere that did not fit adequately the observed line profiles. The rotational velocity and the Gaussian macroturbulence were allowed to vary, while the microturbulence was assumed to be solar ($\sim 0.6 \text{ km s}^{-1}$), negligible, or larger than 1 km s^{-1} , finally keeping the best value from the point of view of the χ^2 criterion between observed and synthetic spectra. A Gaussian profile was used to represent for the instrumental profile.

Uncertainties have been estimated following the algorithm described by Sánchez Almeida (1997):

$$\sigma_k^2 = \alpha_{kk}^{-1} \chi^2 / N \quad (1)$$

where α_{kl} represents the standard covariance matrix, and N is the number of free parameters. That is, errors are evaluated as the standard least-square estimate (see, for instance, Press et al 1988), augmented by the square root of the ratio between the number of data and the number of free parameters. With this correction, uncertainties are reliable even in the case the minimum of χ^2 has not been reached.

3.3. A test of the depth coverage using the solar spectrum

We can make use of the previously studied solar case to estimate the boundaries of the depth coverage reached with the current set of spectral lines. The solar inversion model

was derived from the solar line spectrum in the FTS atlas of Kurucz et al. (1984), with a higher signal-to-noise ratio and spectral resolution than our stellar spectra. The McDonald day-light spectra were acquired with the same spectrograph and similar signal to noise as the stellar spectra, and provide the possibility to carry out a test of the results obtained with the McDonald setup. Thus, we have repeated the application of the MISS code to the solar spectrum, using the 10 lines selected in common for Gmb1830 and ϵ Eri extracted from the McDonald day-light spectra. Fig. 2 shows the retrieved model (solid line: error bars are shown) compared with the solar model obtained from the inversion of 40 lines in the Kurucz et al. (1984) atlas (dashed line), as described in Allende Prieto et al. (1998). The smaller sample of lines narrows the photospheric region covered. Nonetheless, the agreement is reasonable for $-2.5 \geq \log \tau \geq -0.5$, with differences smaller than 200 K suggesting that the ten selected spectral lines map approximately this part of the solar photosphere.

3.4. Derived model photosphere

The derived model stellar photospheres are shown in Fig. 3, and compared with theoretical model photospheres from the grid by Kurucz (1992), and the exact solution to the gray atmosphere ($T^4 = \frac{3}{4}T_{\text{eff}}^4[\tau + q(\tau)]$) of the assigned effective temperatures (see below). The quality of the final fit to the observed line spectra is shown in Fig. 4 for the two stars. There are marked differences between the temperature stratification of the semi-empirical models and their purely theoretical counterparts. While the star’s gravity is determined with high accuracy from the trigonometric parallaxes measured by Hipparcos (Nissen, Høg & Schuster 1997; Allende Prieto et al. 1999b) and some additional hypotheses, the effective temperature typically gives discrepant values when derived from different methods such as photometry, Balmer lines, excitation equilibrium, the spectral energy distribution, or temperature sensitive line ratios. We treat the effective temperature of the

appropriate theoretical model as an unknown parameter. Metallicity influences only weakly the considered spectral features.

The derived rotational velocities are 2.5 and 2.1 km s⁻¹ for Gmb1830 and ϵ Eri, respectively. They compare well with those empirically measured by Fekel (1997): 2.2 and 2.0 km s⁻¹. Mayor and collaborators derived 1.5 km s⁻¹ for ϵ Eri from the CORAVEL measurements (Benz & Mayor 1984), while Gray (1984) gives 2.2 km s⁻¹. Smith et al. (1992) derived 1.8 km s⁻¹ for the combination of the different broadening mechanisms: instrumental, macroturbulence and rotation. However, our rotational velocities should be taken with caution. The inversion code is not able to cleanly unravel the Gaussian macroturbulence from the rotational broadening profile. Moreover, the use of the Van der Waals approximation for the collisional broadening with neutral hydrogen is expected to underestimate, systematically, the collisional broadening, and should produce larger-than-real estimates for the rotation-macroturbulence broadening. The derived Gaussian macroturbulence is 0.0 and 1.5 km s⁻¹ for Gmb1830 and ϵ Eri, respectively, and in both cases the preferred microturbulence was 0.6 km s⁻¹.

Obviously, the abundances obtained directly from the inversion are only those of the elements whose lines are represented in the sample selected as input data. These are: calcium, titanium, chromium, and iron. The results appear in Table 4. The derived ratio of iron to calcium abundances for Gmb1830 agrees very well with that found by Smith et al. (1992) making use of MARCS model atmospheres (Gustafsson et al. 1975), and Balachandran & Carney (1996) making use of those of Kurucz (1992). But the iron abundance with respect to the Sun derived by both groups, is ~ 0.1 dex higher than ours. The comparison of the abundances of these elements in ϵ Eri with the determination by Drake & Smith (1993) shows a discrepancy for calcium of +0.13 dex ($A(\text{Ca}) = 6.26 - 6.39$)⁴

⁴ $A(\text{M}) = \log \left(\frac{N(\text{M})}{N(\text{H})} \right) + 12.$

and a difference of 0.28 dex for iron: our result is $[\text{Fe}/\text{H}] = +0.19$ dex, and theirs was $[\text{Fe}/\text{H}] = -0.09$. These and others inconsistencies found for ϵ Eri (see Drake & Smith (1993) and §5 of this paper) might be partly related to the magnetic activity of the star.

4. Spectroscopic properties of the derived semi-empirical models

We have made use of several spectroscopic indicators to test the depth stratification of the stellar photosphere: the optical spectral energy distribution, weak metal lines spanning a wide range in excitation potential, and collisionally enhanced wings of strong metallic lines. The optical continuum and the excitation balance of weak metal lines are highly sensitive to temperature. The wings of the very few strong metal lines for which detailed theoretical calculations or laboratory measurements of their damping constants is available (Lambert 1993) are reliable estimators of the pressure in the line forming region (see, e.g., Edvardsson 1988, Anstee, O’Mara & Ross 1997). Other tools are available, such as the wings of the Balmer lines (Fuhrmann, Axer & Gehren 1993), but have not been included here because they are more complicate to interpret. The reader is referred to Fuhrmann et al. (1993) for an extensive discussion on the analysis of hydrogen lines.

4.1. Stellar continuum. Optical and UV

While most of the spectrophotometric measurements in the literature do not provide an estimate of their accuracy, the availability of different **independent** determinations allows us to derive empirically their precision for the case of Gmb1830. Figure 5a compares the observed optical fluxes with the models’ prediction normalized at $7500 \text{ \AA} (1/\lambda(\mu\text{m}) \simeq 1.33)$, the reddest wavelength where all the different observational sources have data. Independently observed fluxes are represented by filled circles (Breger 1976), open circles

(Peterson & Carney 1979) and asterisks (Carney 1983). The true continuum (no line blanketing), given the low metallicity of the star, is expected to fall very close to the observed continuum, except in the blue part of the spectrum, where it should be higher, consistent with the presence of many absorption lines. The prediction of the MISS model (solid line) shows this behavior. It is shown in the Figure that, for the fixed gravity and metallicity ($\log g = 4.68$; $[\text{Fe}/\text{H}] = -1.3$), a theoretical model atmosphere with an effective temperature $T_{\text{eff}} \simeq 5050$ K reproduces the observations. This was already pointed out by Balachandran & Carney (1996). The fluxes for the theoretical (Kurucz 1992) models⁵ take into account the presence of lines (unlike the MISS continuum) and are therefore directly comparable with the observations. The effective temperature derived from the optical continuum is consistent, as expected, with that recently derived by Alonso, Arribas, & Martínez Roger (1996) making use of the Infrared Flux Method (IRFM; Blackwell et al. 1990): 5029 K.

The absolutely calibrated UV spectra of Gmb1830 in the IUE final archive (IUEFA) offer us the possibility to carry out an independent test. Combining the apparent brightness of the star in the Johnson V band, $V = 6.42$, and the *Hipparcos* parallax, $\pi = 0.109$ mas, we arrive at an absolute magnitude for this star $M_V = 6.61$. Using this value and the star’s metallicity to choose an isochrone from α -elements enhanced models of Bergbusch & Vandenberg (1992), quite independently of the assumed star’s age due to the fact that the star has not evolved from the main sequence, we find the stellar mass to be $M = 0.64 \pm 0.05 M_{\odot}$, in agreement with the older estimate by Smith et al. (1992), and the stellar radius $R = 0.61 \pm 0.05 R_{\odot}$. The radius and the parallax directly provide the dilution factor of the flux as the light travels from the star to Earth, making it possible to compare models’

⁵These fluxes were obtained through interpolation in the Kurucz’s grid, available at the CCP7 web site: <http://ccp7.dur.ac.uk>.

surface fluxes and the IUE observations. Fig. 5b re-enforces the conclusion previously obtained from the slope of the optical continuum, that the T_{eff} of the theoretical model atmosphere is close to 5050 K. Unfortunately, at the present stage we cannot carry out a detailed spectral synthesis, including the many lines present in this spectral range, with the MISS model. However, it is unclear whether the lines used here for the modeling are able to constrain the layers of the photosphere where the UV continuum is forming.

The optical continuum of ϵ Eri, as appears in Breger’s catalog, has been represented in Fig. 6. Again, the MISS model (solid line) predicts a slope compatible with the observations. The effective temperature for a theoretical model that fits the continuum slope is somewhat hotter than $T_{\text{eff}} \simeq 4850$ K (dashed line), but cooler than 5200 K. Alonso et al. (1996) derived 5076 K, and this is the temperature that we assign to the theoretical models shown in Fig. 3b. We recall that the chromospheric activity of ϵ Eri dominates the UV spectrum of the star, excluding the possibility of studying the photosphere from this spectral region. Using the isochrones of Bergbusch & Vandenberg (1992) we find that ϵ Eri’s mass is $M = 0.76 \pm 0.05 M_{\odot}$, and its radius $R = 0.55 \pm 0.05 R_{\odot}$.

4.2. Weak lines. Excitation equilibrium of Fe I

The highly accurate determinations of the transition probabilities for a large sample of neutral iron lines by O’Brian et al. (1991) provide an independent test of the semi-empirical model. We have identified 12 iron lines in O’Brian et al.’s list within our spectral range, covering a significant range in excitation potential and equivalent width to explore the excitation equilibrium of neutral iron for the considered model atmospheres. The lines are listed in Table 5, with their measured equivalent widths.

The MISS model for Gmb1830, with the derived solar-like microturbulence, does not

exhibit a significant dependence of the derived iron abundance on the equivalent width. The upper panel of Fig. 7 shows the differences between the abundances observed and predicted by MISS, as derived from the differences between observed and predicted equivalent widths. The slope of the linear (least-squares) model is 0.002 ± 0.007 . The lower panel shows that the excitation equilibrium is satisfied: the slope of the derived abundance against excitation potential is 0.012 ± 0.074 .

The Fe I lines in the O’Brian et al’s list identified in the spectrum of ϵ Eri are the same ones observed in Gmb1830, except for λ 5321 Å. Of course, given the higher metallicity, the lines are stronger in this case. Figure 8 shows that the microturbulence retrieved in the modeling process for ϵ Eri induces no significant gradient in the abundance as derived from lines of different strength. The excitation equilibrium is satisfied for this set of lines as well: the slope of the abundance differences as a function of the excitation potential is 0.018 ± 0.045 .

4.3. Wings of strong metallic lines

The wings of the Ca I λ 6162 line were used as input for the semi-empirical modeling, and the spectral region close to the line is very useful as weak calcium lines are present, allowing a test of the retrieved model and calcium abundance. In Fig. 9 (upper panel) the observed spectrum is shown (dots), and compared with the synthesis using the MISS structure (solid line). The MISS model reproduces nicely not only the observed wings of the strong line, as imposed in the modeling process, but also the surrounding calcium and iron lines, with the derived calcium abundance: $A(\text{Ca}) = 5.27$, or $[\text{Ca}/\text{H}] = -1.09$, which is 0.3 dex higher than the derived iron abundance. The result, that fully agrees with the analyses using MARCS model atmospheres by Smith et al. (1992), reflects the well-known over-abundance of α -elements in metal-poor stars. Departures from LTE are expected in

the core of the λ 6162 Å line.

The lower panel of Fig. 9 shows the same spectral region for ϵ Eri. The observed spectrum (dots) is nicely reproduced by the MISS model with $[\text{Ca}/\text{H}] = +0.03$. The oscillator strengths were extracted from the Vienna Atomic Line Database (VALD), and have been tested against the solar spectrum (Allende Prieto et al. 1998).

5. Summary and conclusions

We have applied an inversion method to normalized line profiles in the optical spectra of the metal-poor dwarf Gmb1830 and the solar-metallicity dwarf ϵ Eridani. This demonstrates the viability of the empirical modeling to stars other than the Sun, to which the inversion had been previously applied (Allende Prieto et al. 1998). The semi-empirical models reproduce very well weak-to-moderate lines of neutral atoms, and satisfy the excitation equilibrium of iron. The models also fit the wings of strong lines, and the slope of the optical continuum.

The derived model atmospheres are slightly different from the theoretical models of a similar effective temperature, showing a steeper temperature gradient. These differences must correspond to missing ingredients in the theoretical modeling. In our view, a likely candidate is stellar granulation. The semi-empirical models are one-dimensional, static, and time-independent too, but flux-constancy is no longer imposed. This flexibility provides room for missing physics in the complex dynamical interplay between matter and radiation. Therefore studying and analyzing the differences between theoretical and semi-empirical structures may help us to recognize which physical effects are lacking. The mean temperature structure derived from numerical simulations of solar granulation (Stein & Nordlund 1998) has shown a steeper gradient for the layers outwards than $\log \tau \simeq -0.5$,

resembling the behavior of the semi-empirical models presented here. This effect was also apparent in the semi-empirical model for the solar photosphere we derived using the same technique.

The differences between the semi-empirical model and the flux-constant models for Gmb1830 do not affect significantly the abundances previously published for this star. It is of interest that the absolute abundance of Li measured by Deliyannis et al. (1994) in Gmb1830, namely $A(\text{Li}) = 0.27$ dex, does not change by more than 0.01 dex when using the semi-empirical model for this star.

If departures from LTE are significant, the semi-empirical models would adapt themselves to reproduce the line profiles under LTE. This effect has been named **NLTE masking** and has been invoked to explain the differences between the Holweger & Müller (1974) empirical solar model and solar NLTE models by Rutten & Kostik (1982). Quantifying the importance of departures from LTE should be performed through detailed calculation of model atmospheres. Hauschildt, Allard & Baron (1999) have already stepped forward to this, computing models for the Sun and Vega, but these studies need to be extended to a wide range of physical parameters. At this point, we can take a glimpse at the consistency of the results provided by the inversion procedure checking the iron abundance that comes out from the analysis of ionized iron lines. In late-type dwarfs, such as those analyzed here, most of the iron is in form of Fe^+ ions and therefore, departures from LTE ionization equilibrium are unlikely to disturb the abundances derived from lines of this species. Smith et al. (1992) and Drake & Smith (1993) analyzed four and three Fe II lines in the spectra of Gmb1830 and ϵ Eri, respectively. Using their atomic data, we synthesized the lines with the semi-empirical models and the abundances retrieved from neutral lines, finding that the agreement between observed and predicted equivalent widths for Gmb1830 is excellent, always better than 1 mÅ. Conversely, the equivalent width predicted for the

Fe II lines of ϵ Eri, are systematically smaller than the observations, leading to a higher iron abundance by 0.2 dex than the Fe I lines, which may be an indicator of departures from LTE (we recall that this star exhibits magnetic activity). It is worthwhile to note that Feltzing & Gustafsson (1998) found further evidence of overionization (compared to LTE predictions) for several K dwarfs. Socas-Navarro, Ruiz Cobo, & Trujillo Bueno (1998) have developed a NLTE inversion procedure oriented to the study of the solar chromosphere. The implementation of the method to stars is highly desirable, and its application to ϵ Eri may bring into agreement the abundances of neutral and ionized lines.

Understanding of the atmospheric structure and the line formation in metal-poor stars is of particular relevance. Detailed abundance analyses on these stars provide precious information on the chemical evolution of the Galaxy, how metals are synthesized in stellar interiors, or even the yields of the primordial nucleosynthesis. Very recently, Asplund et al. (1999) have computed the first hydrodynamical simulations of surface convection for metal-poor stars, similar to those of Stein & Nordlund (1998) for the Sun. The mean temperature structures they derive for HD140283 ($[\text{Fe}/\text{H}] \simeq -2.5$) and HD84937 ($[\text{Fe}/\text{H}] \simeq -2.3$) show again a steeper gradient in the layers of $\log \tau \leq -0.5$ than the flux-constant stratification of the corresponding one-dimensional models. This turns out to have important consequences for the derived lithium abundance, indicating that lithium abundances could have been overestimated by 0.2 – 0.35 dex in metal-poor stars using one-dimensional model atmospheres. Data of similar quality to those presented in this paper, and even wider spectral coverage have been collected for HD140283 during the past few years (Allende Prieto et al. 1999a), and should provide an alternative semi-empirical model for this star in the near future.

We thank Martin Asplund, Luis Ramón Bellot Rubio, Manolo Collados, Klaus Fuhrmann, Bengt Gustafsson, and Nataliya Shchukina for fruitful discussions. Suchitra

Balachandran and Bruce Carney have kindly provided measurements of the optical continuum of Gmb1830, and Benjamín Montesinos helped with the IUE data. We are grateful to the staff at McDonald Observatory for their professional support. This research has been partially supported by the NSF (grant AST-9618414), the Spanish DGES (projects PB92-0434-C02-01 and PB95-1132-C02-01), and the Robert A. Welch Foundation of Houston, Texas. NOS/Kitt Peak FTS data used here were produced by NSF/NOAO. We have made use of VALD, the IUE final archive, data from the *Hipparcos* astrometric mission of the ESA, and the SIMBAD database, operated at CDS (Strasbourg, France).

REFERENCES

- Allende Prieto, C., & García López, R. J. 1998, *A&AS*, 129, 41
- Allende Prieto, C., Ruiz Cobo, B., & García López, R. J. 1998, *ApJ*, 502, 951
- Allende Prieto, C., García López, R. J., Lambert, D. L., & Gustafsson, B. 1999a, *ApJ*, in press
- Allende Prieto, C., García López, R. J., Lambert, D. L., & Gustafsson, B. 1999b, *ApJ*, in press
- Alonso, A. Arribas, S., & Martínez-Roger, C. 1996, *A&A*, 117, 227
- Anders, E., Grevesse, N. 1989, *Geochimica et Cosmochimica Acta*, 53, 197
- Anstee, S. D., O'Mara, B. J., & Ross, J. E. 1997, *MNRAS*, 284, 202
- Asplund, M., Nordlund, Å, Trampedach, R., & Stein 1999, *A&A*, 346, L17
- Balachandran, S. C., & Carney, B. W. 1996, *AJ*, 111, 2
- Beardsley, W. R., Gatewood, G., & Kamper, K. W. 1974, *ApJ*, 194, 637
- Benz, W., & Mayor, M. 1984, *MNRAS*, 270, 499
- Blackwell, D. E., & Shallis, M. J 1979, *MNRAS*, 186, 669
- Blackwell, D. E., Petford, A. D., Arribas, S., Haddock D. J. & Selby M. J. 1990, *A&A*, 232, 396
- Bergbusch, P. A., & Vandenberg, D. A. 1992, *ApJS*, 81, 163
- Breger, M. 1976, *ApJS*, 32, 7
- Carney, B. W. 1983, *AJ*, 88, 623
- Deliyannis, C. P., Ryan, S. G., Beers, T. C., & Thorburn, J. A. 1994, *ApJ*, 425, L21
- Drake, J. J., & Smith, G. 1993, *ApJ*, 412, 797

- Edvardsson, B. 1988, A&A, 190, 148
- Fekel, F. C. 1997, PASP, 109, 514
- Feltzing, S., & Gustafsson, B. 1998, A&AS, 129, 237
- Fuhrmann, K. Axer, M., & Gehren, T. 1993, A&A, 271, 451
- Garhart, M. P., Smith, M. A., Levay, K. L., & Thompson, R. W. 1997, IUE NSIPS
Information Manual, v2.0, IUE Nasa Newsletter, No. 57
- Gray, D. F. 1980, ApJ, 235, 508
- Gray, D. F. 1984, ApJ, 277,640
- Gray, D. F., & Baliunas, S. L. 1995, ApJ, 441, 436
- Greaves, J. S., Holland, W. S., Moriarty-Schieven, G., Jenness, T., Dent, W. R. F.,
Zuckerman, B., McCarthy, C., Webb, R. A., Butner, H. M., Gear, W. K., & Walker,
H. J. 1998, ApJ, 506, L133
- Griffin, R. F. 1984, Observatory, 104, 192
- Gustafsson, B., Bell, R. A., Eriksson, K., & Nordlund, Å. 1975, A&A, 42, 407
- Gustafsson, B., & Jørgensen, U. G. 1994, A&A Rev., 6, 19
- Hauschildt, P. H., Allard, F., & Baron, E. 1999, ApJ, 512, 377
- Heintz, W. D. 1984, PASP, 96, 557
- Holweger, H. & Müller, E. A. 1974, Solar Phys., 39, 19
- Kurucz, R. L., Furenlid, I., Brault, J., & Testerman, L. 1984, NOAO Atlas No. 1, The
Solar Flux Atlas from 296 to 1300 nm (Sunspot, NM: National Solar Observatory)
- Kurucz, R. L. 1992, private communication
- Lambert, D. L. 1993, Phys. Scr., T47, 186
- Mäcke, R., Holweger, H, Griffin, R., & Griffin, R. 1975, A&A, 38, 239

- Magain, P. 1985, *A&A*, 146, 95
- Meylan, T., Furenlid, I., Wiggs, M. S., Kurucz, R. L. 1993, *ApJS*, 85, 163
- Nissen, P. E., Høg, E., & Schuster, W. J. 1997, in *Proceedings of the ESA Symposium Hipparcos - Venice 97*, ESA SP-402, 225
- O'Brian, T. R., Wickliffe, M. E., Lawler, J. E., Whaling, W., & Brault, J. W. 1991, *J. Opt. Soc. Am. B*, 8, 1185
- Peterson, R. C., & Carney, B. W. 1979, *ApJ*, 231, 762
- Press, W.H., Flannery, B.P., Teukolsky, S.A., & Vetterling, W.T. 1988, *Numerical Recipes* (Cambridge: Cambridge Univ. Press)
- Radick, R. R., Lockwood, G. W., Skiff, B. A., & Baliunas, S. L. 1998, *ApJS*, 118, 239
- Ruland, F., Holweger, H., Griffin, R., Griffin, R., & Biehl, D. 1980, *A&A*, 92, 70
- Rutten, R. J., & Kostik, R. I. 1982, *A&A*, 115, 104
- Ryan, S. G. 1998, *A&A*, 331, 1051
- Sánchez Almeida, J. 1997, *ApJ*, 491, 993
- Smith, G., Lambert, D. L., & Ruck, M. J. 1992, *A&A*, 263, 249
- Socas-Navarro, H., Ruiz Cobo, B., & Trujillo Bueno, J. 1998, *ApJ*, 507, 470
- Spielfiedel, A., Feautrier, N., Chambaud, G., & Lévy, B. 1991, *J. Phys. B*, 24, 4711
- Stein, R. F., & Nordlund, Å. 1998, *ApJ*, 499, 914
- Thatcher, J. D., Robinson, R. D., & Rees, D. E. 1991, *MNRAS*, 250, 14
- Tull, R. G., MacQueen, P. J., Sneden, C., & Lambert, D. L. 1995, *PASP*, 107, 251
- Wilson, O. C. 1978, *ApJ*, 226, 379

Fig. 1.— Variation of the iron abundance through the inversion process for Gmb1830, starting from different initial estimates.

Fig. 2.— The solar MISS model atmosphere (Allende Prieto et al. 1998; dashed line), derived using 40 spectral lines in the Kurucz et al. (1984) atlas, compared with the model retrieved from the McDonald Observatory day-light spectrum using only the 10 lines in this study for Gmb1830 and ϵ Eri (solid line with error bars).

Fig. 3.— a) The semi-empirical model for Gmb1830 (solid line), compared with a model computed with ATLAS9 for $T_{\text{eff}} = 5050$ K (dashed) and $T^4 = \frac{3}{4}T_{\text{eff}}^4[\tau + q(\tau)]$ (Gray atmosphere) b) Semi-empirical and flux-constant models for ϵ Eri.

Fig. 4.— a) Fit of the observed line profiles (dots) in the spectrum of Gmb1830 with the semi-empirical model (dashed line); b) the same for the spectrum of ϵ Eri. The dots correspond to all the wavelengths which are actually fitted by the inversion procedure, joined together, regardless of the existence of gaps between the different segments corresponding to a single spectral line, or one of the wings of a spectral line.

Fig. 5.— a) Normalized optical continuum of Gmb1830; data from Breger (1976): filled circles; Peterson & Carney (1979): open circles; and Carney (1983): asterisks. The *true* continuum predicted by the MISS model (solid line) and the *blanketed* continua of the Kurucz’s models for $T_{\text{eff}} = 4900, 5050,$ and 5300 K are also shown. b) Near UV continuum of Gmb1830 observed by IUE (dots). The continua of the Kurucz’s models for $T_{\text{eff}} = 4900, 5050,$ and 5300 K are also shown.

Fig. 6.— Normalized optical continuum of ϵ Eri; data from Breger (1976): filled circles. The *true* continuum predicted by the MISS model (solid line) and the *blanketed* continua of the Kurucz’s models for $T_{\text{eff}} = 4650, 4850,$ and 5200 K are also shown.

Fig. 7.— Differences between the abundances observed and predicted by the MISS model for Gmb1830, as derived from the difference in the equivalent widths of Fe I lines in the O’Brian et al’s list, against observed equivalent widths (upper panel) and excitation potential (lower panel). Also shown are linear regressions (least squares) indicating no dependence of the abundances on these parameters.

Fig. 8.— Same as Fig. 7, but for ϵ Eri.

Fig. 9.— The region of the Ca I λ 6162 Å for Gmb1830 (upper panel) and ϵ Eri (lower panel), compared with the MISS model synthesis (solid line). The core of the Ca I λ 6162 line is likely to be seriously affected by departures from LTE.

Table 1. Observations: Dates, Spectral Ranges and Signal-to-noise Ratios.

Star	Spectral range (\AA)	Date	SNR
ϵ Eri	4851-6402	29-Feb-96	700
”	5204-7183	27/29-Feb-96	800
Gmb1830	4853-6404	26-Feb-96	250-350
”	5204-7183	27/29-Feb-96	300-400

Table 2. Large Aperture Low Dispersion spectra available in the IUE Final Archive for Gmb1830

IUEFA Image	Acquisition Date	Exposure time (s)
LWR07351	30-Mar-80	120.000
LWR07471	10-Apr-80	999.708
LWP05802	23-Apr-85	359.506
LWP13413	12-Jun-88	252.000

Table 3. Spectral lines used in the inversion

Element	Wavelength ^a (Å)	Exc. Pot. (eV)	$\log gf$
Ca I	6166.445*	2.52	-1.142
Ca I	6499.642*	2.52	-0.818
Ca I	6162.166*	1.89	-0.097
Ti I	5490.165	1.46	-0.877
Ti I	6258.101*	1.44	-0.299
Cr I	5312.872*	3.45	-0.562
Cr I	5300.743*	0.98	-2.129
Fe I	5225.524*	0.11	-4.790
Fe I	5956.711*	0.86	-4.610
Fe I	6151.614*	2.18	-3.300
Fe I	6173.352	2.22	-2.880
Fe I	6750.149*	2.42	-2.620

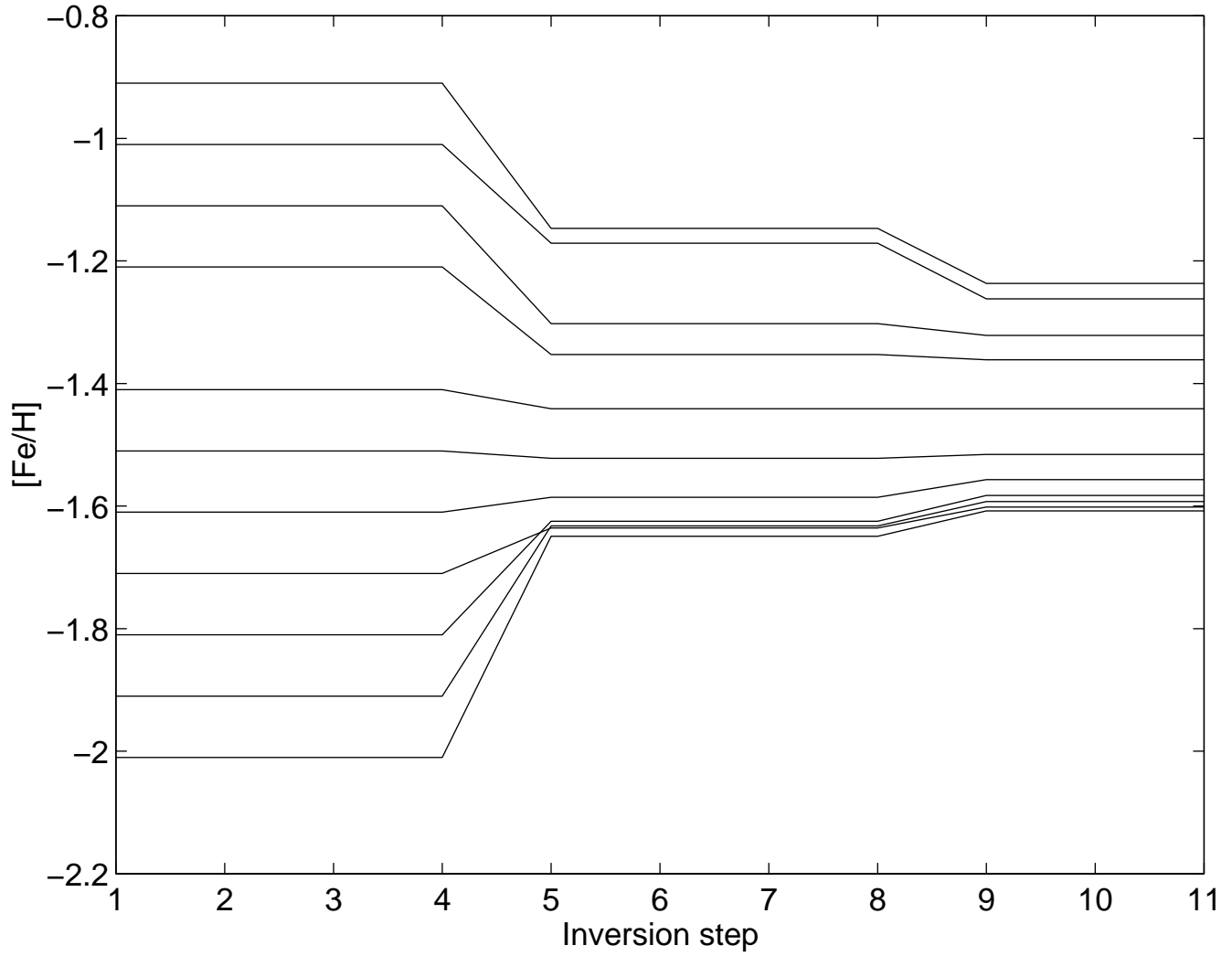
^aThe lines used for modeling ϵ Eri are identified with an asterisk

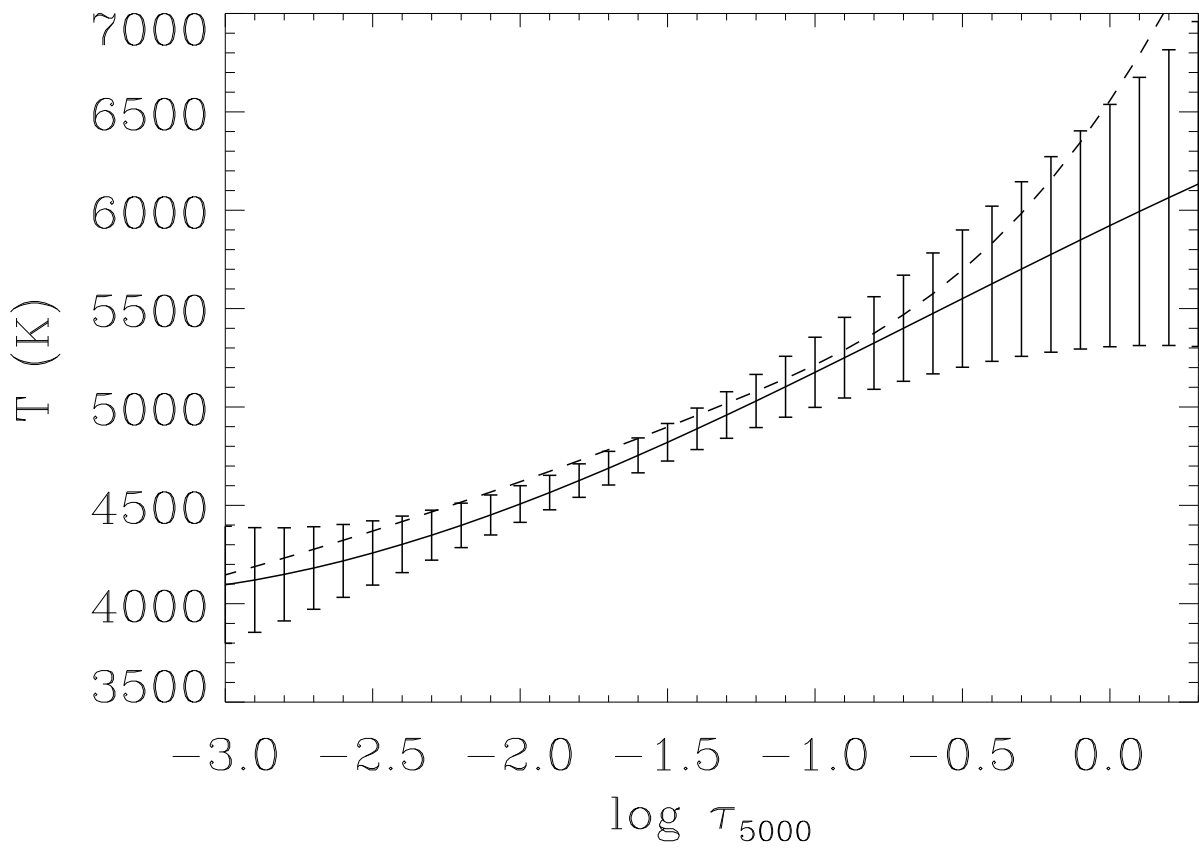
Table 4. Abundances derived from the inversion

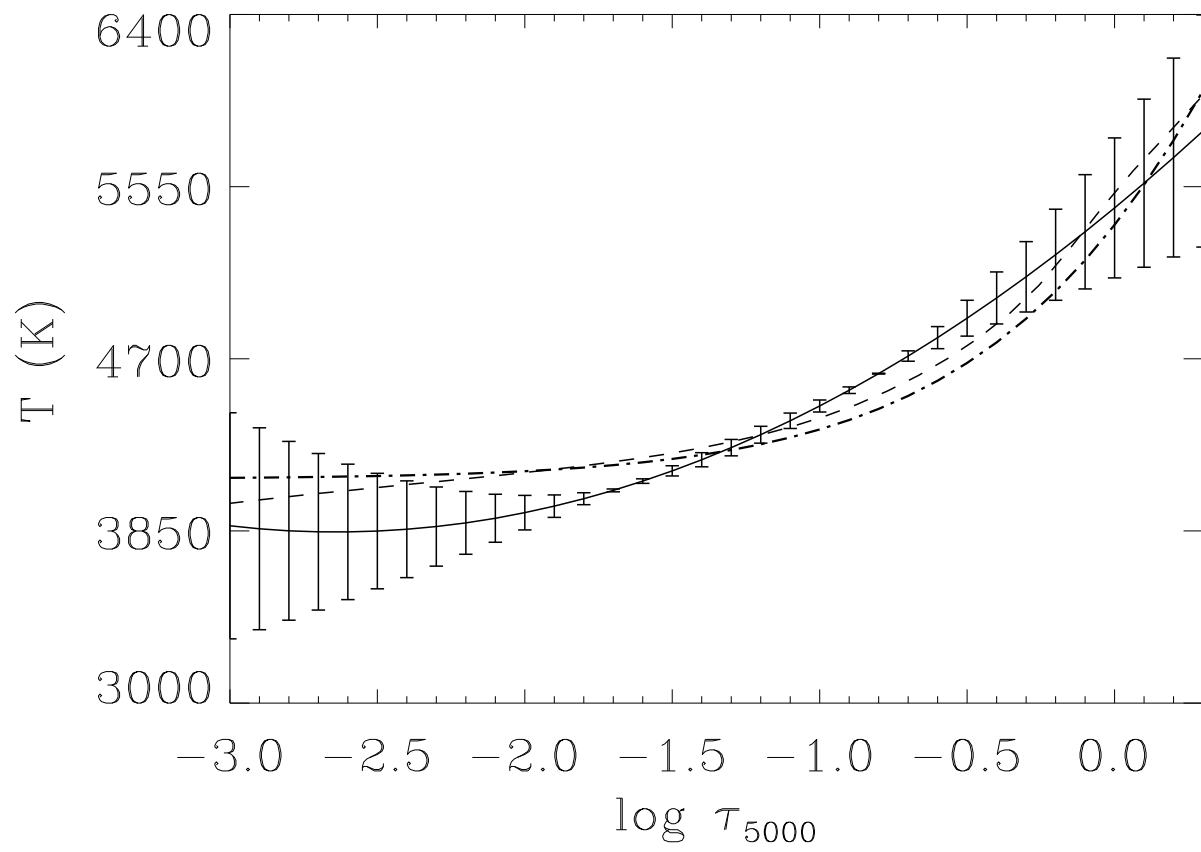
Star	Element	Num. of lines	Abundance	[M/H]
<i>Gmb</i> 1830	Fe	7	6.09	−1.39
”	Ca	3	5.27	−1.09
”	Ti	3	3.78	−1.09
”	Cr	2	4.26	−1.41
ϵ Eri	Fe	6	7.67	+0.19
”	Ca	3	6.39	+0.03
”	Ti	2	4.80	−0.19
”	Cr	2	5.73	+0.06

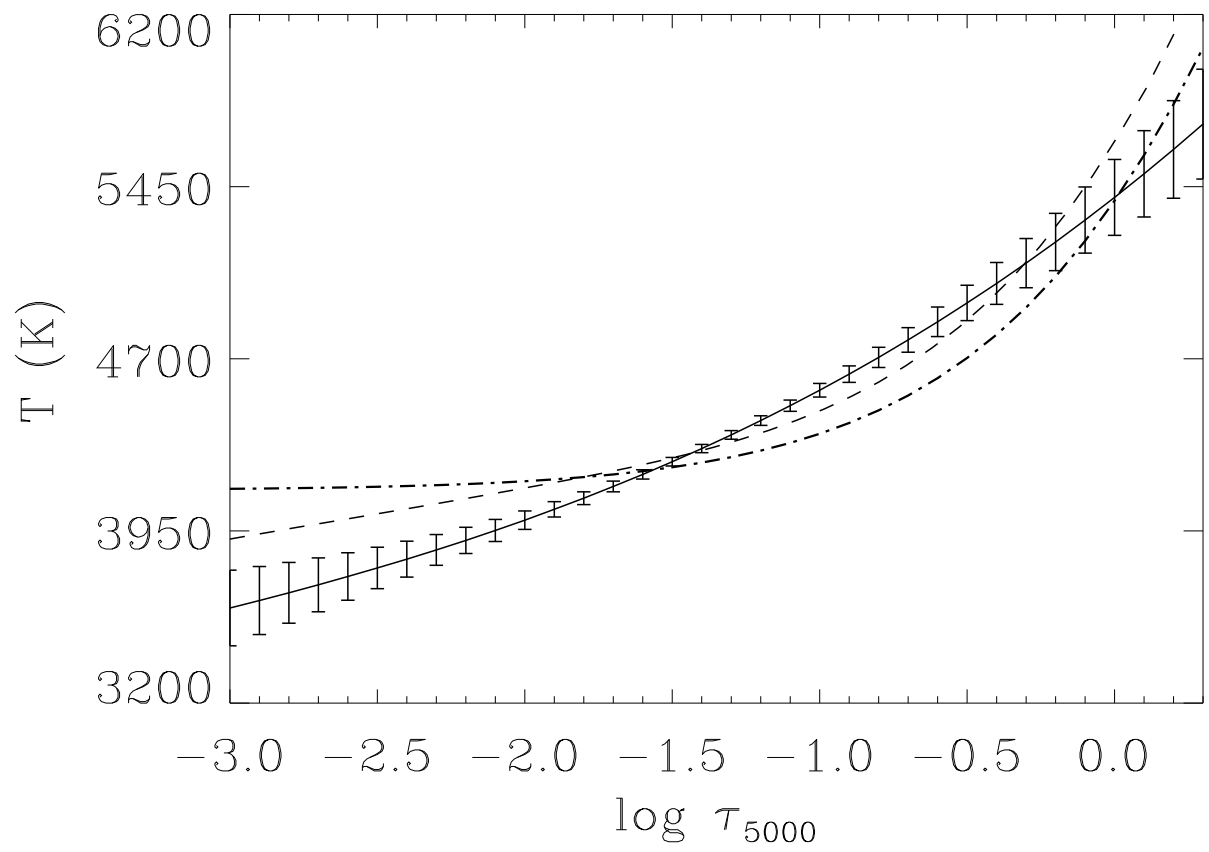
Table 5. Measured Fe I lines in the list of O’Brian et al. (1991)

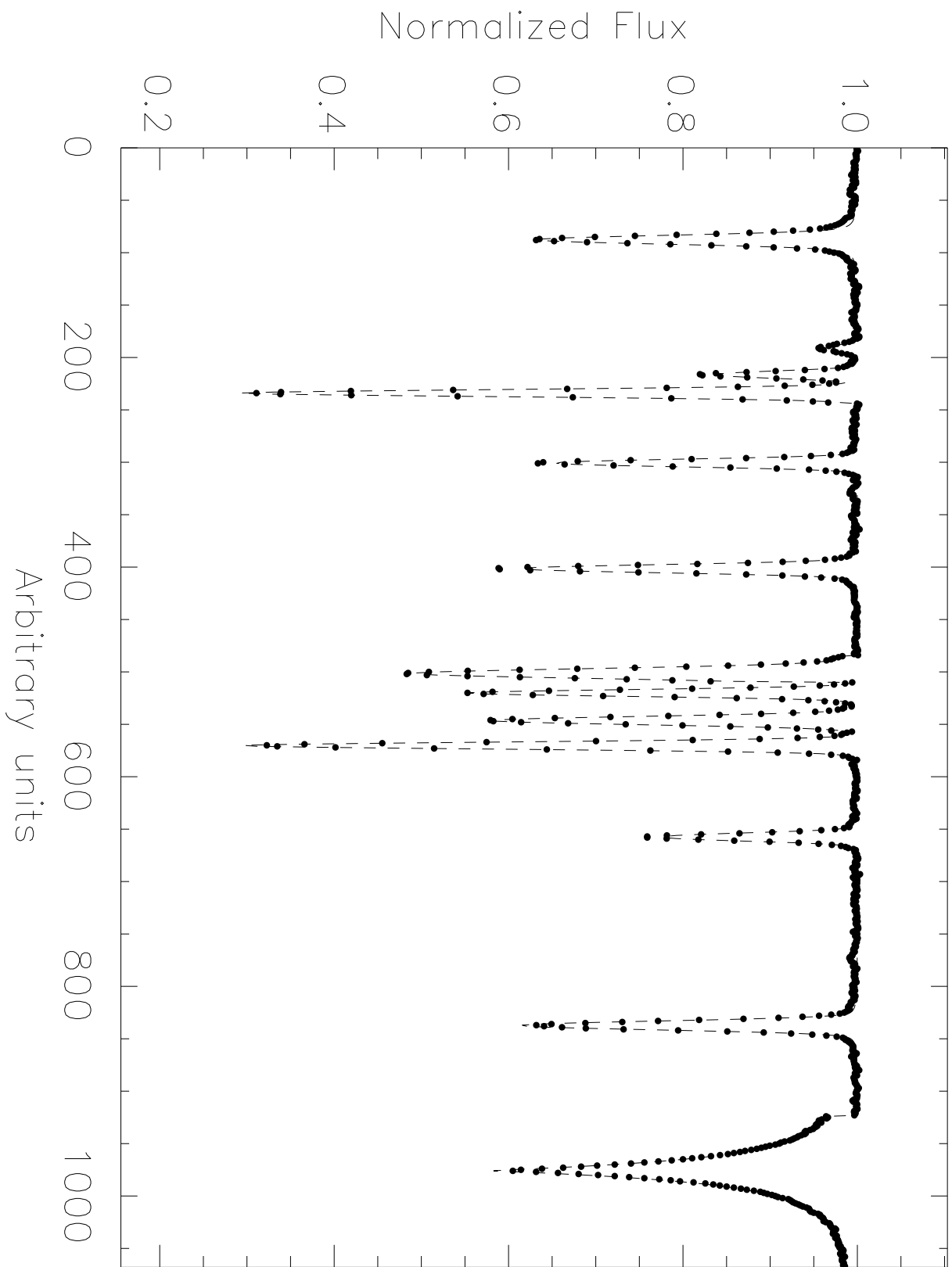
Wavelength (Å)	Exc. Pot. (eV)	$\log gf$	W_λ Gmb1830 (mÅ)	$W_\lambda \epsilon$ Eri (mÅ)
5223.18	3.63	−1.78	7.6	40.5
5225.52	0.11	−4.76	60.7	110.5
5321.11	4.43	−1.09	10.6	...
5856.08	4.29	−1.33	6.2	43.1
5956.71	0.86	−4.50	32.1	83.8
6165.35	4.14	−1.47	10.6	58.2
5288.53	3.69	−1.51	18.9	67.4
5379.58	3.69	−1.51	21.2	73.6
5464.28	4.14	−1.40	10.4	46.8
6151.61	2.18	−3.37	23.4	72.8
6498.95	0.96	−4.69	25.8	78.1
6750.14	2.42	−2.58	44.6	103.1

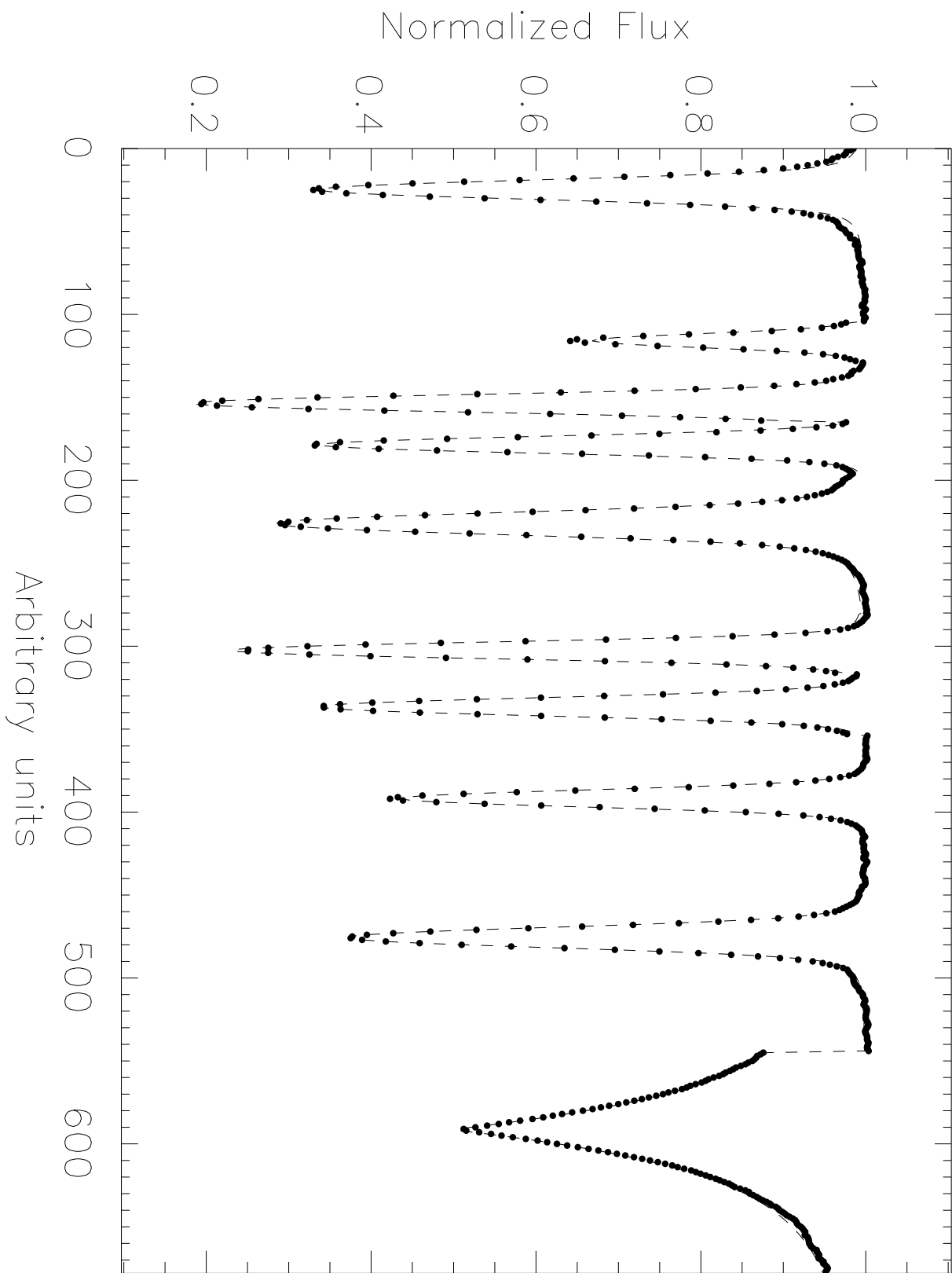




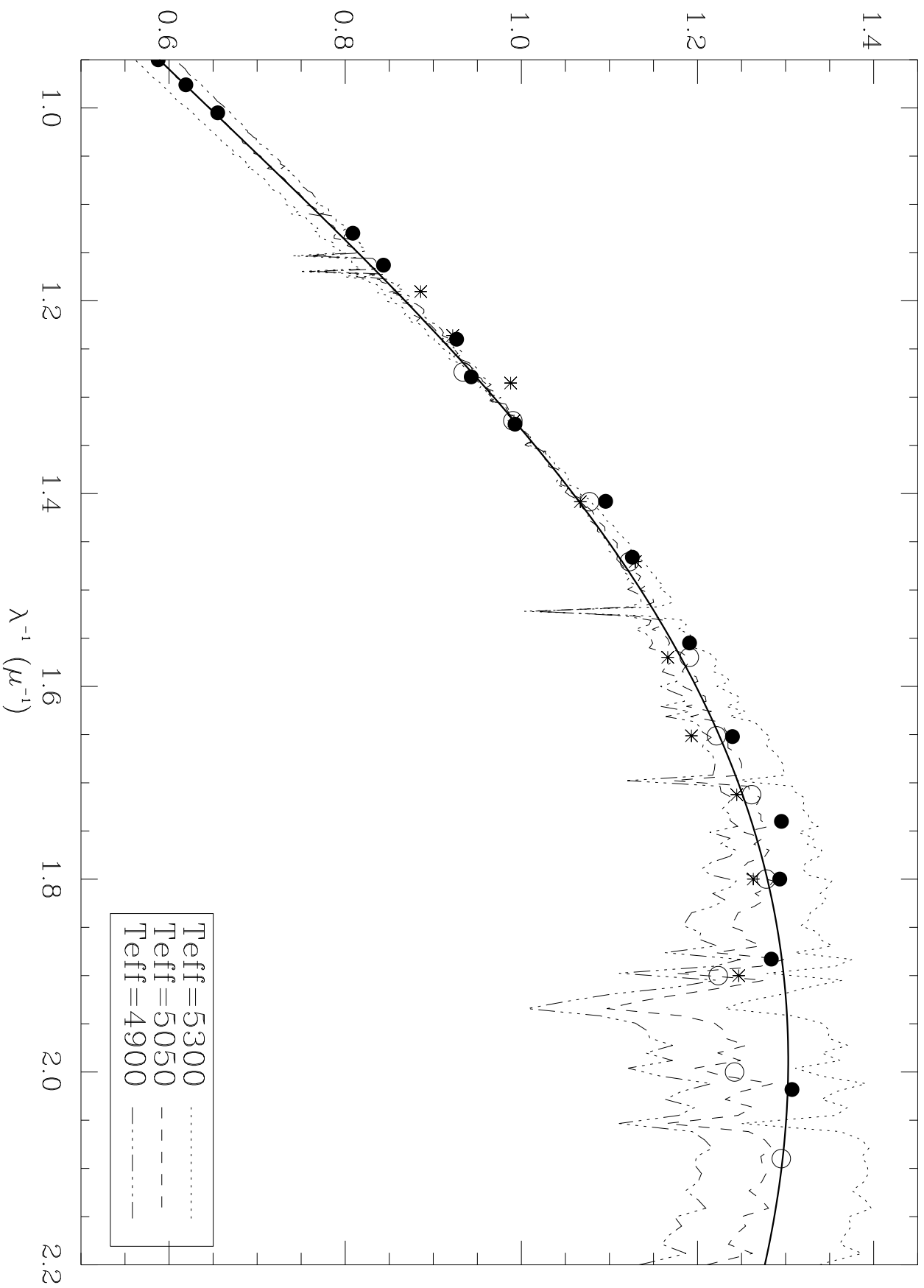


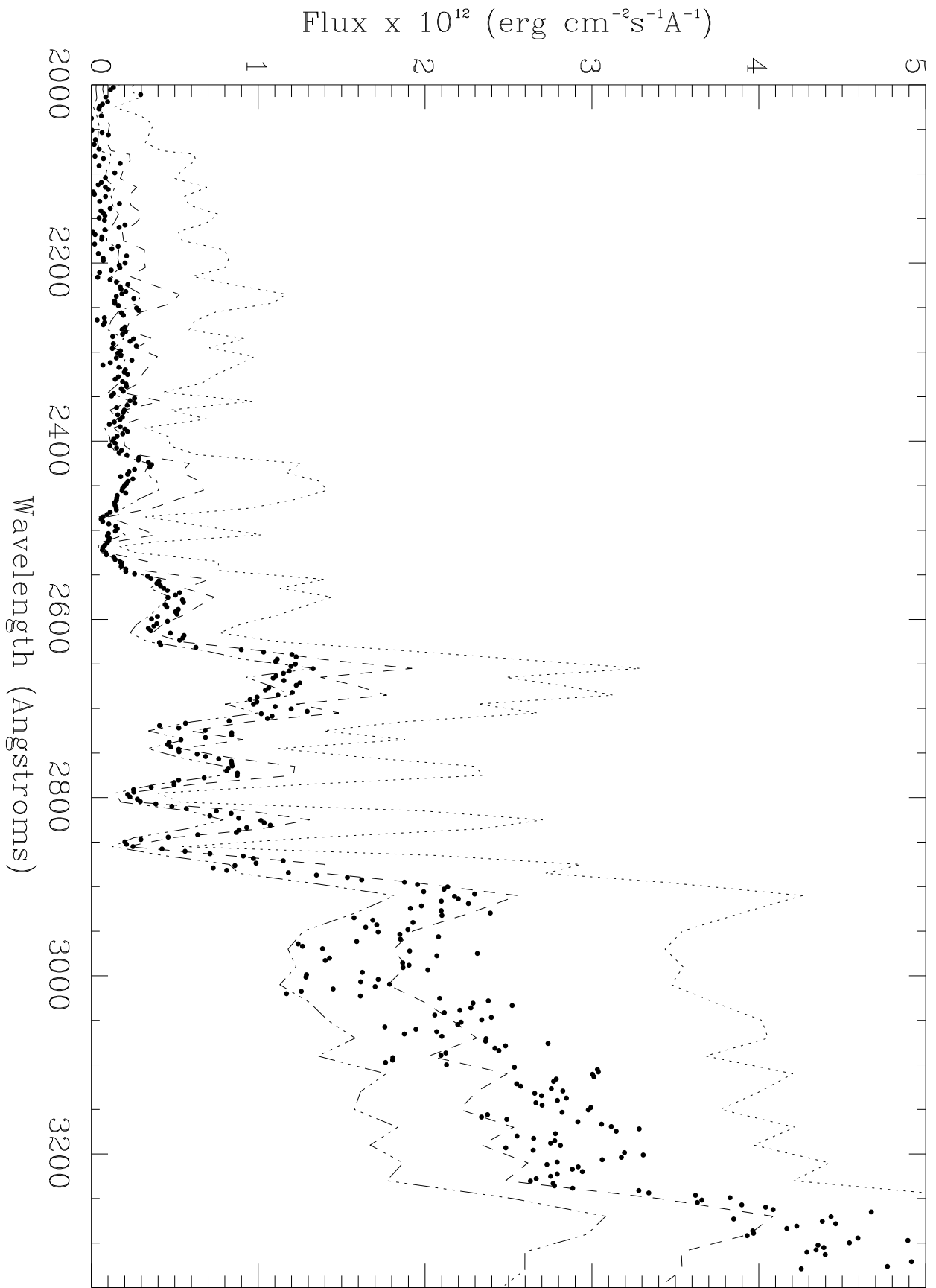






Gmb 1830





e Eri

